Pol. J. Environ. Stud. Vol. 22, No. 5 (2013), 1307-1316

Original Research

Kinetic and Thermodynamic Studies for Phosphate Removal Using Natural Adsorption Materials

Eva Chmielewská*, Renata Hodossyová, Marek Bujdoš

Faculty of Natural Sciences, Comenius University, Mlynská dolina B2,
842 15 Bratislava, Slovak Republic

Received: 2 January 2013
Accepted: 11 February 2013

Abstract

Batch adsorption experiments were carried out to study the kinetics and thermodynamics of phosphate removal from model solutions on the surfaces of some selected adsorbents. The data obtained were analyzed using two reaction-based kinetic models and a diffusion-based model. In order to examine the extent to which diffusion participates in this adsorption process, the data were processed by the Weber-Morris mass transfer model. The Freundlich model represented a slightly better description of phosphate adsorption onto slovakite and GEH^{104} than onto clinoptilolite-rich tuff, while the Redlich-Peterson model yields a better fit for phosphate adsorption onto clinoptilolite-rich tuff. Adsorption onto montmorillonite proceeds best using the Sips isotherm model. The calculated $\Delta G°$ values show that under standard conditions the adsorption of phosphate onto all adsorbents examined occurs spontaneously.

Keywords: clinoptillolite-rich tuff, oxyhydroxide GEH, montmorillonite, slovakite, adsorption, kinetic and thermodynamic properties, phosphate removal from water

Introduction

Industrial, agricultural, and mining activities are the reason why most of our water bodies suffer from superfluous concentrations of phosphorus and thus eutrophication and water quality deterioration. Currently, many physico-chemical techniques like chemical precipitation, membrane processes, and filtration and coagulation for phosphate removal are available. However, they suffer from many disadvantages like high cost, salt content in the effluent, necessities of chemical sludge disposal, etc. The biological method applied in wastewater treatment technology, like intracellular bacterial polyphosphates accumulation, is very sensitive to wastewater composition and ambient temperature (BOD toward total phosphorus content and the presence of light degradable hydrocarbons, including luxury uptake microflora, i.e. actynomycetes). In recent years, research and production of alternative adsorbents that may potentially replace the costly commercial adsorbents has intensified in water cleanup processes [1-5].

In this paper some attention is focused on the various traditional adsorbents in a few of the local repositories, which prove enhanced performance for environmental pollutants removal. Due to their low cost and local availability, natural materials such as zeolite, montmorillonite, industrial waste product, chitosan, low-rank coal lignite, dolomite, clay, and iron oxyhydroxides were chosen to evaluate their adsorption performance in phosphate removal. Except for those inexpensive natural adsorbents, some opportunities for hybrid organic-inorganic materials and multifunctional design adsorbents is emerging in water decontamination. Many of these strategies are evident in biological materials. Thus, they are inspiring exciting new directions in materials design and synthesis based on the

*e-mail: chmielewska@fns.uniba.sk

molecular level, using soft and biomimetic materials, simultaneously. The process of natural biomaterials implementation for the intensive improvement of the adsorption properties of traditional materials is advantageous, in hierarchy over the ordinary adsorption, as published in the literature [6-9].

Natural zeolites have been the most popular, inexpensive, and alternative adsorbents in water cleanup for several decades. According to Babel et al. [4], they are 15-times cheaper than the other worldwide broaden natural product chitosan. On the other hand, if the chitosan starts to be used more often for water treatment as coated or as host substance in embedded hybrid adsorbents, this product may significantly improve its removal performance, profitability, and economic feasibility, including its considerable price decrease. By such a strategy the environment also may benefit. Nevertheless, the low-cost adsorbents, in general, may in near future contribute to the more efficient protection and sustainability of our environment [9-16].

Materials and Methods

Adsorbents Examined

Al-Mg – montmorillonite-rich bentonite originated from the deposit Stará Kremnička – Jelšový Potok in the Slovak Republic, which is the most popular and long mined ore of the country. Bentonite from this ore meets most of the geotechnical requirements for the construction of the filler, damping, and sealant barriers. Basically, bentonite belongs to a group of natural nanomaterials composed predominantly of crystalline mineral particles from the group of dioctahedral smectites – montmorillonite (less than 0.2 mm). In contact with water and polar liquids bentonite allows us to expand in volume up to 12 or more times and in such a plastic state keeps viscous, desirable rheological properties with the typical sealing effects. Montmorillonite, from montmorillonite-rich bentonite, was obtained after sedimentation and purification procedures [16-20]. The price of the montmorillonite on the market costs 30-80 Euro per ton [4, 20]. Its surface area S(BET) reaches the value 240 m^2/g, and the bulk density of montmorillonite is about 2.0 g/cm^3.

Natural zeolites, mostly clinoptilolite-rich tuffs of Slovak, United States (Castle Creek, Idaho), and Chinese (Hubei) deposits, as well as mordenite from New Zeland, were examined. The domestic natural clinoptilolite (Nižný Hrabovec repository in eastern Slovakia) was chosen on the basis of its low-price in the local market (15-35 Euro per ton for size-granulation of 0.3-1 mm), cost-effectivness, and its sufficiently large surface area (~ 60 m^2/g), the highest among the other natural products, rigidity, and surface functionality. However, the huge Chinese zeolite producer Shijiazhuang Mining Imp & Exp Trade Co. offers clinoptilolite-rich tuffs according to pretreatment for 30-215 Euro per ton. Natural zeolite in USA is purchased for 20-80 Euro per ton [4, 18]. Zeolites are crystalline, hydrated aluminosilicates with a typical system of structural cages and channels. The common physical characteristics of this clinoptilolite-rich tuff are the following: bulk density 2.39 g/cm^3, shipping weight 0.84 g/cm^3, total porosity of about 35%, size – granulation of 0.2-0.5 mm [10, 17, 18].

Granulated ferric hydroxide ($GEH^{102,104}$) was developed at the Department of Water Quality Control in Technical University of Berlin in the early 1990s for removal of arsenic from natural waters and is an approved commercial adsorbent manufactured by GEH Wasserchemie GmbH & Co. KG Osnabrück (Germany). The main components of GEH are akaganeite (ß-FeOOH) and goethit [α-FeO(OH)]. The product has the specific surface area of about 220 m^2/g, water content of 45%, bulk density 1.2 g/cm^3, and a price of 3,750 Euro per ton. For the experiments the size granulation under 0.3 mm was selected [19].

Slovakite decodes a commercial adsorbent manufactured by IPRES Inžiniering, Ltd. Bratislava from domestic dolomite, bentonite, diatomic clays, alginite, and zeolite, justified only with clinker and final pressurizing. This product received EU Patent No. 1098851. Slovakite is purchased for about 700 Euro per ton in the size granulation of 0.2-0.5 mm. The bulk density of this product equals 2.1 g/cm^3 and S(BET) surface to 23 m^2/g [17].

Alginite fossil (in size granulation of 0.2-0.5 mm, with the specific surface area of 27 m^2/g) was from the southeastern Slovak deposit Pinciná [7]. Alginite is an ecological raw material that originates from the algae stock deposition (*Botryococcus braunii* Ktz.) situated at the bottom of a maar lake together with the clay weathering, products washed out from the maar ring, and composed of the basalt tuffs. This fossil possesses high humus content, macro-, micronutritive and trace elements, including considerable dehydration ability what supports its utilization as soil fertilizer, pharmaceutical additive, and environmental adsorbent. The bulk density of this fossil equals 0.85 g/cm^3 and porosity is higher than by the other natural aluminosilicates (45%). Alginite price per ton on the market oscillates around 30-40 Euro per ton [4, 7, 15].

Calsit, as a molecular sieve of synthetic zeolite type 5A, having a pore size of 0.5 nm, was manufactured by Research Institute for Oil and Petroleum Gases in Slovnaft Bratislava (Slovak Republic). Calsit, with about 70% of Na ions exchanged into Ca ions, has bulk density of 0.7 g/cm^3, the maximum water content in granulated form of 1.5% wt, porosity about 40%, and specific surface area of 353 m^2/g [6]. Before experiments, the cylindrical extrudates with the diameter of 3.0 mm were mechanically powderized to get some comparable size granulation of 0.2-0.5 mm with the other used adsorbents.

Chinese blast furnace slag (industrial solid waste) originated from a coal (thermal) power station in the broader vicinity of Shanghai. According to the elemental analysis performed, the slag consisted of amorphous predominantly calcium aluminosilicate. Slag obtained was characterized by the size granulation of less than 0.2 mm. Bulk density of the slag is 2.4 g/cm^3 and its surface area S(BET) equals 11 m^2/g. Blast furnace slag used to be purchased in China for 28 Euro per ton [4].

Combined chitosan-zeolite adsorbent was prepared at the Technical University of Liberec (Czech Republic) in the

nanospider apparatus, which ensured more or less an electrostatic inclusion of self-organized chitosan chains into zeolitic channels.

Chitosan (a chelating scavenger of heavy metals) is produced from chitin, which is the second most abundant natural biopolymer (after cellulose) on the globe,. It is made by alkaline N-deacetylation of chitin, widely found in the exoskeleton of shellfish and crustaceans such as crab, lobster, insects, mushrooms, and bacteria. High adsorption performance of chitosan to toxic metals is attributed to the large number of hydroxyl- and aminogroups including chitosan flexible polymer chain structure [1, 17]. Bulk density and surface area S(BET) of this chitosan-zeolite adsorbent were comparable to the raw zeolite samples, except the porosity parameter, which was slightly lowered due to the covering of the external surface of this product with the chitosan chains.

Analytical Procedures

Chemicals necessary for the stock solution preparation were purchased mostly from Lachema Brno (made in Czech Republic) of analytical grade quality. Aqueous model solutions of the pollutant examined in adsorption experiments (as phosphate) were determined by means of Isotachophoresis on a ZKI 02 analyzer (Villa Labeco). The measured data were processed by ITP PRO 32 program (Kas Comp, Ltd. Bratislava). Atomic Emission Spectrometry (ICP OES, Jobin Yvon 70 Plus) at the wavelength 213,618 nm for phosphorus was also used for experimental results verification.

Laboratory Setup

A continuous and well mixed batch reactor used to be the most common way to study the reaction between solute and adsorbent. This experimental configuration offers a number of potential advantages like long contact time, upon which a high particle load may be derived or controlled mixing to reduce an external mass transfer effect.

Batch mode or discontinuous adsorption experiments were carried out using the 30 mL aliquot of model solution with variable pollutant concentration and 0.3 g adsorbents (weight with analytical precision) equilibrated for the designated time interval in 100 mL glass stopper bottles, after which the supernatant solutions were separated mostly by centrifugation and such rezidual pollutants analyzed. The samples were agitated in a horizontal Elpan water bath shaker equipped with variable speed and water bath temperature adjustment, necessary for the thermodynamic (3 various temperatures) measurements. All the batch experiments were thus carried out at constant temperature in a shaking water thermostat by agitation speed of 200 rpm.

The initial phosphate concentration in the solutions examined during the kinetic and thermodynamic studies were always identical, used the prepared stock solution (Co ~ 300 mg/L), whose concentration was permanently verified with analytical precision at the begining of every experiment. All measurements were done in triplicate.

The equilibrium uptake capacity a (in mg/g) for each sample was calculated according to the following mass balance equation:

$$a_{eq} = \left(\frac{C_i - C_{eq}}{m} \right) V$$

...where C_i and C_{eq} were initial and equilibrium concentrations of studied pollutant (in mg/L), m was the mass of adsorbent examined (in g), and V was volume of the solution in liters (L).

To compare the bounding strengths of the adsorbed phosphate on the four best adsorbents examined, i.e. clinoptilolite-rich tuff, GEH, montmorillonite, and slovakite, some simple test for reversed elution of phosphate into 1% NH_4Cl solution was realized. Before this elution test, all those adsorbents were loaded with phosphate by identical procedure in aqueous solutions of 100 g PO_4^{3-}/L (10 g of adsorbent in 1 L of solution) using the laboratory shaking machine for 4 hours. Such phosphate-loaded adsorbents were then separated and thoroughly washed in deionized water to remove surface, weakly bound phosphate, and dried at 105ºC for 2 hours in a laboratory drier.

Results and Discussion

Kinetic Studies

The adsorption dynamic is traditionally described by the following three consecutive steps: transport of the solute from bulk solution through liquid film on the adsorbent exterior surface, solute diffusion into the pores of the adsorbent and parallel the intraparticle transport, and adsorption of the solute into the interior surface of the adsorbent [8, 11-13].

Various kinetic models have been suggested for adsorption, including the Lagergren pseudo-first and pseudo-second order, external diffusion, or intraparticle diffusion (Weber-Morris mass transfer) models, expressed in Eqs. 1-5 below [8-14]:

$$\log\left(a_{eq} - a\right) = \log a_{eq} - \frac{k_1}{2.303} t \qquad (1)$$

$$\frac{t}{a} = \frac{1}{k_2 a_{eq}^2} + \frac{1}{a_{eq}} t \qquad (2)$$

$$a = k_i \sqrt{t} + C \qquad (3)$$

$$D_f = 0.23 \frac{r_o \delta a_{eq}}{\sqrt{t}} \qquad (4)$$

$$D_p = \frac{0.03 r_o^2 a_{eq}}{\sqrt{t}} \qquad (5)$$

...where: k_1, k_2, and k_i are the pseudo-first order, pseudo-second order rate constants and rate parameter of the intra-

particle diffusion control stage, respectively; a_{eq} the maximum amount of solute adsorbed at equilibrium in mg/g; a the amount of solute on the surface of the adsorbent at any time t in mg/g; C is the intercept at the ordinate; D_f and D_p are the film and pore diffusion; r_o is radius of sample grains in cm; δ is the film thickness in cm; and t is time in minutes.

Firstly, kinetic measurements presented in Fig. 1 were done to distinguish the phosphate removal performance of the rather broad range, mostly aluminosilicate adsorption materials of the more or less natural-based solids, among which only the most effective ones for the next, more detailed kinetic and thermodynamic studies, were chosen. The data at all curves (Fig. 1) mean the arithmetic average values of three parallel measured samples, usually for every time interval till the equilibrium. While triplicate measurements are statistically indicated only at isotherm plots, they were performed in all experiments despite not recording at the other plots. Experimental kinetic data obtained were computed using the QtiPlot program of non-linear regression analysis.

The study of phosphate adsorption dependence with time onto various adsorption materials was carried out at 298, 313, and 333 K for solutions with Co ~ 300 mg/L and the original pH value 8.8-9. As seen from the curves in Figs. 1 and 2, the adsorption takes place in two steps.

The first step occurs at the beginning stages of adsorption, when phosphate uptake increases rather sharply from the begining of the ordinates. Following that is the second step, which characterizes the entire remaining adsorption of phosphate, gradually up to equilibrium stage. Such two-step adsorption is usually observed in many systems and can be explained as follows: The first step is the adsorption occurring at the external surface of the adsorbent, where a high number of free adsorption sites is available. The second step occurs at a slower rate, since at that stage the diffusion within the porous adsorbents structure proceeds.

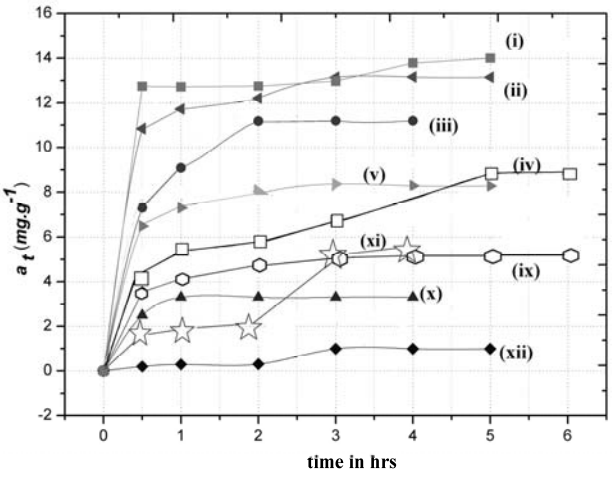

Fig. 1. Adsorption kinetics for phosphate onto different adsorbents at ambient temperature [montmorillonite (i), GEH^{104}(ii), slovakite (iii), Slovakian clinoptilolite-rich tuff (iv), GEH^{102}(v), alginite (ix), calsit (x), chitosan-zeolite composite (xi), Chinese slag (xii)] (Co ~ 300 mg/L).

The data from Fig. 2 were analyzed using two reaction-based kinetic models and a diffusion-based model listed in Table 1. The first reaction-based model is described by Lagergren's first-order rate equation ("pseudo-first-order rate equation") whose integrated form presents Eq. (1). The second reaction-based model applied is described by the pseudo-second-order rate equation, whose integrated form yields expression (2).

Application of two models on the adsorption of phosphate onto 4 types of adsorbents showed that both possess satisfactory agreements as judged by the values of the determination coefficients. However, the analysis of the temperature dependence of the rate constants suggests that the pseudo-second-order model offers a more realistic description of the phosphate adsorption kinetics than Lagergren's first-order model (Table 1).

In order to examine the extent to which diffusion participates in this sorption process, the data were further processed by the Weber-Morris mass transfer model [13-15, 22-24]. This model was described by the above rate equation (3). Fig. 2 presents plots of a vs. $t^{1/2}$ for three various temperatures and 4 adsorbents, whereas the result of the corresponding linear regression analysis is summarized in Table 1. Based on the plots at Fig. 2, the fictive straight lines obtained consist usually of two segments: the first segment, occurs in the $t^{1/2}$ region up to about 5 $min^{1/2}$, while the second one corresponds to higher $t^{1/2}$ values. The first seg-

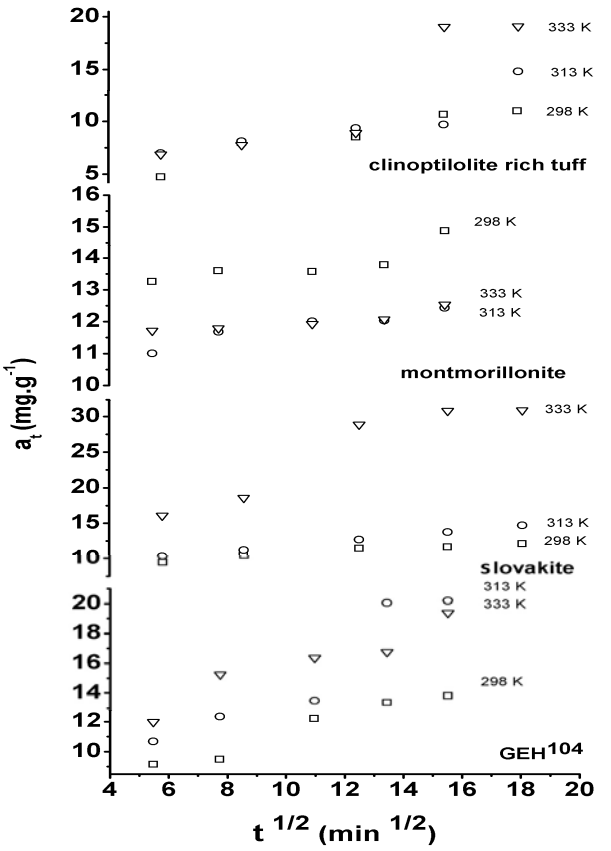

Fig. 2. Intra-particle diffusion kinetic plots for the adsorption of phosphate onto clinoptilolite-rich tuff, montmorillonite, slovakite, and GEH^{104} for three different temperatures (Co ~ 300 mg/L).

ment, with a sharper slope, can be attributed to the diffusion of the phosphate ions through the bulk solution to the externel surface of the adsorbent, i.e. the boundary layer (film) diffusion. The second segment of the fictive lines at Fig. 2 reflects the further gradual adsorption stage, which used to be characteristic for the intraparticle diffusion of pollutant (currently phosphate ions) into adsorbents channels and vacancies. Thus, there are two processes that affect the rate of phosphate adsorption onto clinoptilolite-rich tuff, slovakite, montmorillonite, and GEH[104] adsorbents, but only one of them is a rate-limiting step in the entire process. The slope of each linear portion indicates the rate of the corresponding adsorption, a lower slope describing a slower adsorption process. Based on the results shown in Fig. 2, it follows that film diffusion proceeds faster (at the beginning stage) than the intraparticle-diffusion (at later stages), whereas the second segment of the fictive lines describing intra-particle diffusion does not pass through the ordinate´s origin (C > 0, Table 1). This fact means that the intraparticle diffusion is not the rate-limiting or dominant step in this adsorption process, although proceeding over a longer time period and/or surface reaction adsorption mechanism takes place as the relevant rate-limiting step [8, 14, 22, 24, 26].

Film and pore diffusion equations (Eq. (4) and Eq. (5)) were used furthermore to check whether the film or pore diffusion step controls the adsorption process in the above study. According to Michelson et al. [24], D_f values should be in the range of 10^{-6} to 10^{-8} $cm^2 \cdot s^{-1}$ for film diffusion to be the rate-limiting factor. Similarly, D_p values should be in the range of 10^{-11} to 10^{-13} $cm^2 \cdot s^{-1}$ for pore diffusion to be a rate-limiting factor. Based on our results listed in Table 1 it can be concluded that film-diffusion is the rate-limiting step in all of the adsorbents examined, which simultaneously confirms the results of the applied Weber-Morris mass transfer model.

Standard Free and Activation Energies of the Systems Studied

The variation of the rate constant (obtained from the second-order model, Table 1) with temperature in the 298-333 K region was used for the calculation of the activation energy of adsorption in that region [25-27]. The activation energy was calculated using the Arrhenius equation (6):

$$k_2 = Ae^{-\frac{E_a}{RT}} \tag{6}$$

...where A ($g \cdot mg^{-1} \cdot min^{-1}$) is the Arrhenius pre-exponential factor, E_a ($kJ \cdot mol^{-1}$) is the activation energy, and R ($8{,}314 \cdot 10^{-3}$ $kJ \cdot mol^{-1} \cdot K^{-1}$) is the universal gas constant.

Expression (6) can be rewritten as:

$$\ln k_2 = \ln A - \frac{Ea}{RT} \tag{7}$$

The plot of $\ln k_2$ vs. 1/T using the k_2 values from Table 1 in the 298-333 K range for only the clinoptilolite-rich tuff and slovakite is presented in Fig. 3. From the slope of the

Table 1. The kinetic and thermodynamic values for the adsorption of phosphate ions onto 4 adsorbents in the range of 298-333 K, including selected activation energy E_a data.

Adsorbent	T (K)	Weber-Morris mass transfer model			Lagergren's first-order rate constants		Pseudo-second order rate constants				Film and pore diffusion					
		k	C	R^2	k_1	R^2	k_2	a_{max}	R^2	E_a	D_f	D_p	$\Delta G°$	K_d	ΔH	ΔS
		($mg \cdot g^{-1} \cdot min^{1/2}$)	($mg \cdot g^{-1}$)		(min^{-1})		($g.mg^{-1} \cdot min^{-1}$)	($mg \cdot g^{-1}$)		($kJ \cdot mol^{-1}$)	($cm^2 \cdot s^{-1}$)	($cm^2 \cdot s^{-1}$)	(KJ/mol)	($dm^3 \cdot kg^{-1}$)	(KJ/mol)	KJ/mol·K
Clinoptilolite rich tuff	298	0.587	2.32	0.9077	1.16	0.9772	0.094	11.0	0.9833	13.89	$5.71 \cdot 10^{-6}$	$2.6 \cdot 10^{-5}$	-9.9	55.1	20.8	0.10
	313	0.653	2.85	0.7837	1.18	0.8519	0.092	14.8	0.8871		$7.69 \cdot 10^{-6}$	$3.5 \cdot 10^{-5}$	-11.7	89.1		
	333	1.384	2.36	0.8282	0.14	0.8498	0.001	19	0.8511		$9.87 \cdot 10^{-6}$	$4.5 \cdot 10^{-5}$	-13.9	153.9		
GEH[104]	298	0.522	6.05	0.9555	1.79	0.9638	0.170	13.8	0.9835	–	$7.17 \cdot 10^{-6}$	$3.27 \cdot 10^{-5}$	-10.8	78.2	15.1	0.08
	313	0.625	9.30	0.9004	2.17	0.9785	0.159	19.4	0.9874		$1.00 \cdot 10^{-5}$	$4.60 \cdot 10^{-5}$	-14.1	161.9		
	333	1.037	4.33	0.8937	1.07	0.9149	0.052	20.2	0.9401		$1.04 \cdot 10^{-5}$	$4.79 \cdot 10^{-5}$	-13.5	179.9		
Montmorillonite	298	0.128	12.40	0.7022	5.90	0.9929	1.550	14.9	0.9947	–	$7.74 \cdot 10^{-6}$	$3.53 \cdot 10^{-5}$	-11.0	85.6	- 5.3	0.01
	313	0.124	10.50	0.8982	4.77	0.9983	1.230	12.4	0.9995		$6.44 \cdot 10^{-6}$	$2.94 \cdot 10^{-5}$	-10.9	65.0		
	333	0.073	11.20	0.8400	6.80	0.9976	2.780	12.5	0.9986		$6.49 \cdot 10^{-6}$	$2.96 \cdot 10^{-5}$	-11.6	66.1		
Slovakite	298	0.258	8.27	0.9463	3.04	0.9925	0.467	12.1	0.9990	– 53.2	$8.98 \cdot 10^{-6}$	$5.85 \cdot 10^{-5}$	-10.3	63.4	104.9	0.3
	313	0.438	7.90	0.9994	2.45	0.9720	0.257	14.7	0.9897		$1.09 \cdot 10^{-5}$	$7.11 \cdot 10^{-5}$	-11.7	88.9		
	333	1.668	7.34	0.9017	1.13	0.9802	0.032	30.9	0.9824		$2.29 \cdot 10^{-5}$	$1.49 \cdot 10^{-4}$	-26.1	12 376		

straight line (Ea/R = 1.545×10^4 K), the value of Ea = 13.89 kJ·mol^{-1} for clinoptilolite-rich tuff and of Ea =-53.2 kJ·mol^{-1} for slovakite were obtained, for GEH[104] and montmorillonite the values are not published due to their unaceptable low R^2, using the similar calculation methods. The activation energy value offers some information on whether the adsorption is mainly physical or chemical. The physisorption process has normal activation energy of 5-40 kJ·mol^{-1}, while chemisorption is in the range 40-800 kJ·mol^{-1}. Based on our results, energetically lower surface physisorption of phosphate onto clinoptilolite-rich tuff, GEH, and montmorillonite, but the chemisorption by slovakite was confirmed.

The data obtained from the adsorption experiments at 298, 313, and 333 K, and the initial phosphate concentration of about 300 mg/L were used for calculation of other thermodynamic parameters – standard free energy (Gibbs free energy), ΔG°, and standard entropy from the following equations:

$$\Delta G^0 = -RT \ln K_d \quad (8)$$

$$\Delta G^0 = \Delta H^0 - T\Delta S^0 \quad (9)$$

$$\ln K_d = \left(\frac{\Delta S^0}{R}\right) - \left(\frac{\Delta H^0}{RT}\right) \quad (10)$$

The equilibrium constant K_d was calculated as the ratio of the equilibrium concentrations of phosphate on the adsorbents and in the solutions at constant temperature. The plot of ln K_d vs. 1/T offers a straight line (Fig. 4) and the values of ΔS^o and ΔH^o may be obtained from its intercept and slope, respectively. The calculated thermodynamic parameters (8, 9, 10) for all the tested adsorbents are presented in Table 1. The $\Delta G°$ values listed in Table 1 show that under standard conditions the adsorption of phosphate onto all adsorbents examined occurs spontaneously. The results of standard free energies listed in Table 1 indicate that the spontaneity slightly decreases with temperature.

Isotherm Studies

Fig. 1 depicts adsorption capacity of several commonly used adsorbents in phosphate vs. time dependence, among which the best performing GEH[104] (granular iron oxyhydroxide), montmorillonite, and slovakite exhibit. Nevertheless, Slovakian clinoptilolite-rich tuff showed some quantitative comparable uptake capacity, even without any pretreatment procedure that usually enhances total cost of such a purchased product. The highest phosphate removal performance of domestic natural zeolite among the other foreign zeolite samples (American, Chinese, and New Zealand mordenite) was the reason why we chose Slovakian clinoptilolite rich tuff together with GEH[104], montmorillonite and slovakite for isotherm studies.

Table 2 and Figs. 5-8 present adsorption results on clinoptilolite-rich tuff, GEH[104] product, slovakite, and montmorillonite using the statistical least square method (MW XP, Microsoft Office Excel 2003, regression analysis). The equilibrium data from Figs. 5-8 have been analyzed by two and three parameters empirical isotherm models according to Langmuir (11), Freundlich (12), Sips – Langmuir/Freundlich (13), and Redlich/Peterson (14, 15), which indicated acceptable fits with the parameters listed in Table 2.

$$\frac{1}{a} = \left(\frac{1}{a(\max).b.c(eq)}\right) + \left(\frac{1}{a(\max)}\right) \quad (11)$$

$$a = K.c(eq)^{\frac{1}{n}}$$

$$\text{or} \quad \log a = \log K + \frac{1}{n}\log c(eq) \quad (12)$$

$$a = a_{\max}.\frac{K_{LF}.c^n(eq)}{1+K_{LF}.c^n(eq)} \quad (13)$$

$$a = a_{\max}.\frac{K_{RP}.c(eq)}{1+K_{RP}.c^n(eq)} \quad a = \frac{A\,C(eq)}{1+BC(eq)^g} \quad (14)$$

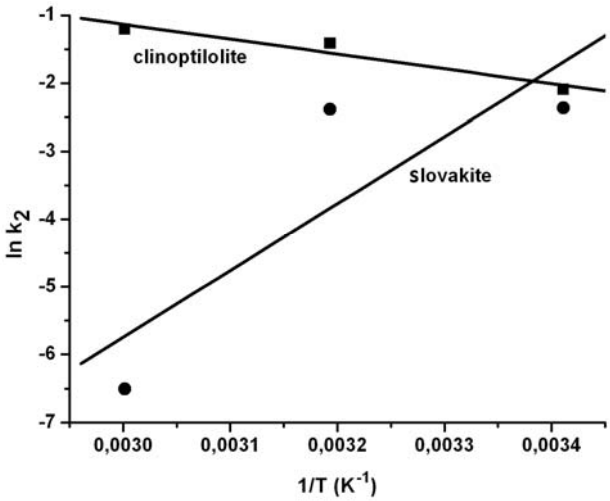

Fig. 3. The Arrhenius plot of ln k_2 vs. 1/T using the k_2 values from Table 1 in the 298-333 K range for clinoptilolite-rich tuff and slovakite (Co ~ 300 mg/L).

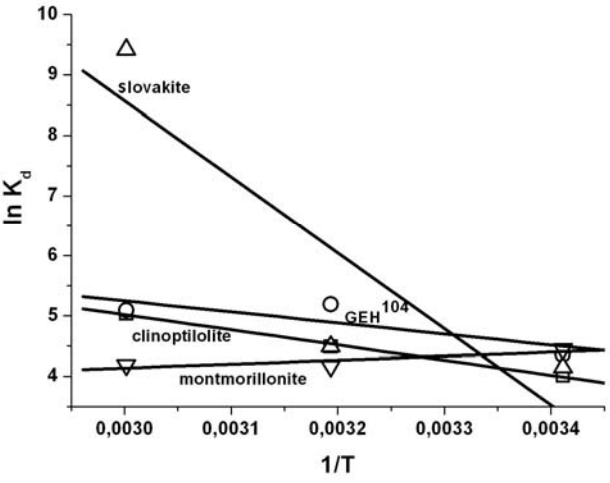

Fig. 4. The plot of ln K_d vs. 1/T for adsorbents studied at 298 K.

Table 2. The isotherm constants and determination coefficients of isotherm models for phosphate adsorption at ambient temperature and selected adsorbents.

Adsorbent	Linear regression						Non-linear regression						
	Freundlich			Langmuir			Redlich-Peterson				Sips		
	K_F	n	R^2	a_{max}	K_L	R^2	g	A	B	R^2	K_S	a_{max}	R^2
Clinoptilolite rich tuff	-	-	-	-	-	-	0.9660	0.064	0.006	0.9830	0.0119	13.8	0.9308
GEH[104]	4.321	4.9	0.9894	14.1	0.252	0.9051	-	-	-	-	-	-	-
Montmorillonite	0.002	0.8	0.9530	-	-	-	-0.0349	$845 \cdot 10^3$	$703 \cdot 10^5$	0.9901	0.00004	58.9	0.9919
Slovakite	1.486	3.0	0.9439	12.4	0.023	0.9021	-	-	-	-	-	-	-

$$\ln\left(A\frac{C(eq)}{a}-1\right)=g\ln C(eq)+\ln(B) \qquad (15)$$

...where a means the specific adsorption capacity, a(max) the maximum adsorption capacity in mg/g, c(eq) the equilibrium concentration in solution in mg/L, and b relates to the affinity of the solute for the binding sites expressed in L/mg. K_{LF}, K_{RP} means Langmuir/Freundlich or Redlich/Peterson coefficient, A, B, C, g – non linear regression constants.

As can be seen from R^2 (determination coefficient) values, the Freundlich and Langmuir models provide a slightly better description of phosphate adsorption onto slovakite and GEH[104] product than onto clinoptilolite-rich tuff (Table 2). Adsorption of phosphate onto the clinoptilolite-rich tuff proceeds better according to the Redlich-Peterson model using the non-linear regression computation. Nevertheless, using the same computation, the adsorption of phosphate onto montmorillonite fits with the highest determination coefficient to the Sips (Langmuir/Freundlich) isotherm model.

Phosphate adsorption onto clinoptilolite-rich tuff proceeds mostly by the surface accessible extra-framework cations Ca^{2+} and Mg^{2+} (in less extent Fe^{3+}, Ba^{2+}), thus undergoing phosphate precipitation, whereas adsorption onto GEH product proceeds probably by linkage of phosphate to cationic Fe^{3+} of iron oxyhydroxide (Fig. 9a-b). Phosphate adsorption onto slovakite is asumed to proceed by linkage of phosphate to plenty of alkalic earth cations present in its natural dolomite and clay constituents and, finally, montmorillonite may adsorb phosphate moreover based on its sufficient interlamellar distance (about 1.2 nm compared to the ionic diameter of PO_4^{3-} 1,196 nm) also by intercalation mechanism (Fig. 9c-d) [20, 28-31].

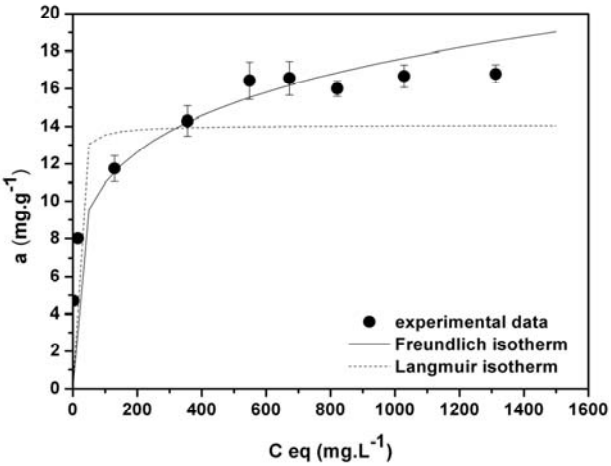

Fig. 6. The isotherms for phosphate adsorption onto GEH[104] product at ambient temperature.

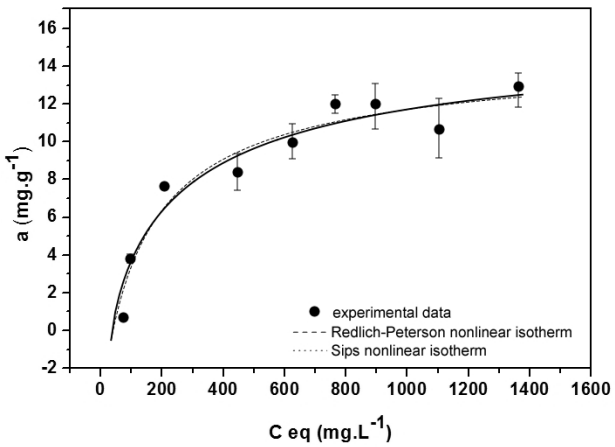

Fig. 5. The isotherms for phosphate adsorption onto clinoptilolite-rich tuff at ambient temperature.

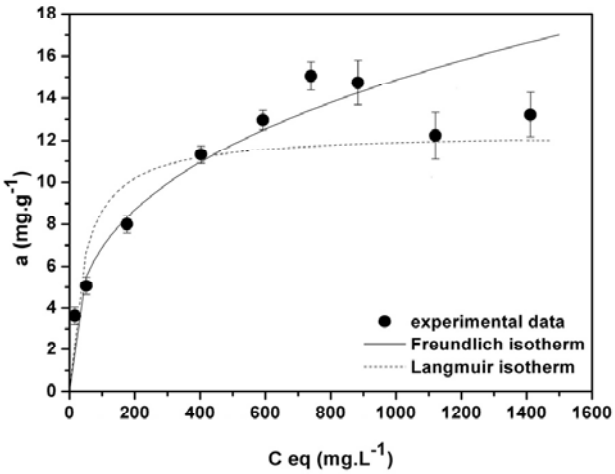

Fig. 7. The isotherms for phosphate adsorption onto slovakite at ambient temperature.

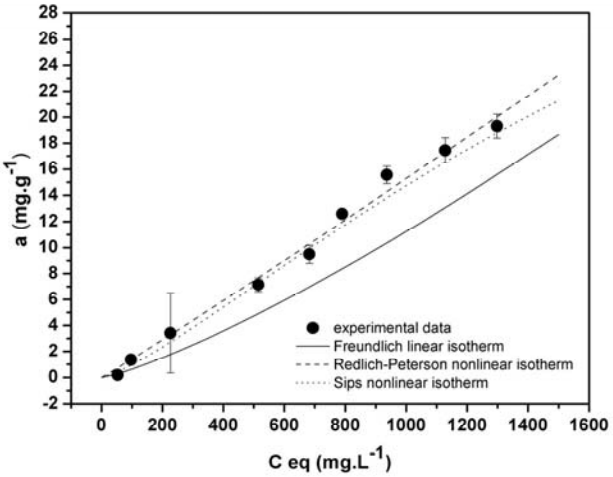

Fig. 8. The isotherms for phosphate adsorption onto montmorillonite at ambient temperature.

To assess the adsorption performance of Chinese slag, synthetic type A Zeolite-Calsit, chitosan-zeolite product, and clinoptilolite- and mordenite-rich tuffs, as well as montmorillonite toward phosphate, the following assumptions may be emphasized. Comparing the pore dimensions of the synthetic A-zeolite (Calsit) (0.42×0.22 nm) with the pure clinoptilolite, whose framework contains narrow 4- and 5-membered SiO_4^{4-} and AlO_4^{5-} tetrahedral rings as well as broad 8- and 10-membered tetrahedral rings constituting intraframework micropores (channels) of 0.33×0.46 nm, 0.3×0.76 nm, and 0.26×0.47 nm enriched by mobile H_2O molecules, moreover, to the ionic diameter of non-hydrated PO_4^{3-} 1.196 nm [6, 29, 30], only interlamellar space of the montmorillonite structure (interlayer distance of about 1.2 nm [20, 31]) approaches the above dimensions and thus potentially supports the phosphate intercalation mechanism by this process studied (Fig. 9c). It must be pointed out simultaneously that volcanic rock of clinoptilolite type contains due to the presence of other minerals overgrowing the active matrix thoroughly (volcanic glass, feldspar, cristobalite, clay, quartz), much broader external pore openings and various interparticle voids, which probably work as phosphate scavengers, too. Based on the S(BET) analysis performed, the BJH average pore diameters of above natural clinoptilolite and mordenite samples were determined in the range 9.2-20 nm [17, 18]. Mordenite structures posses even slightly broader pore openings than clinoptilolite

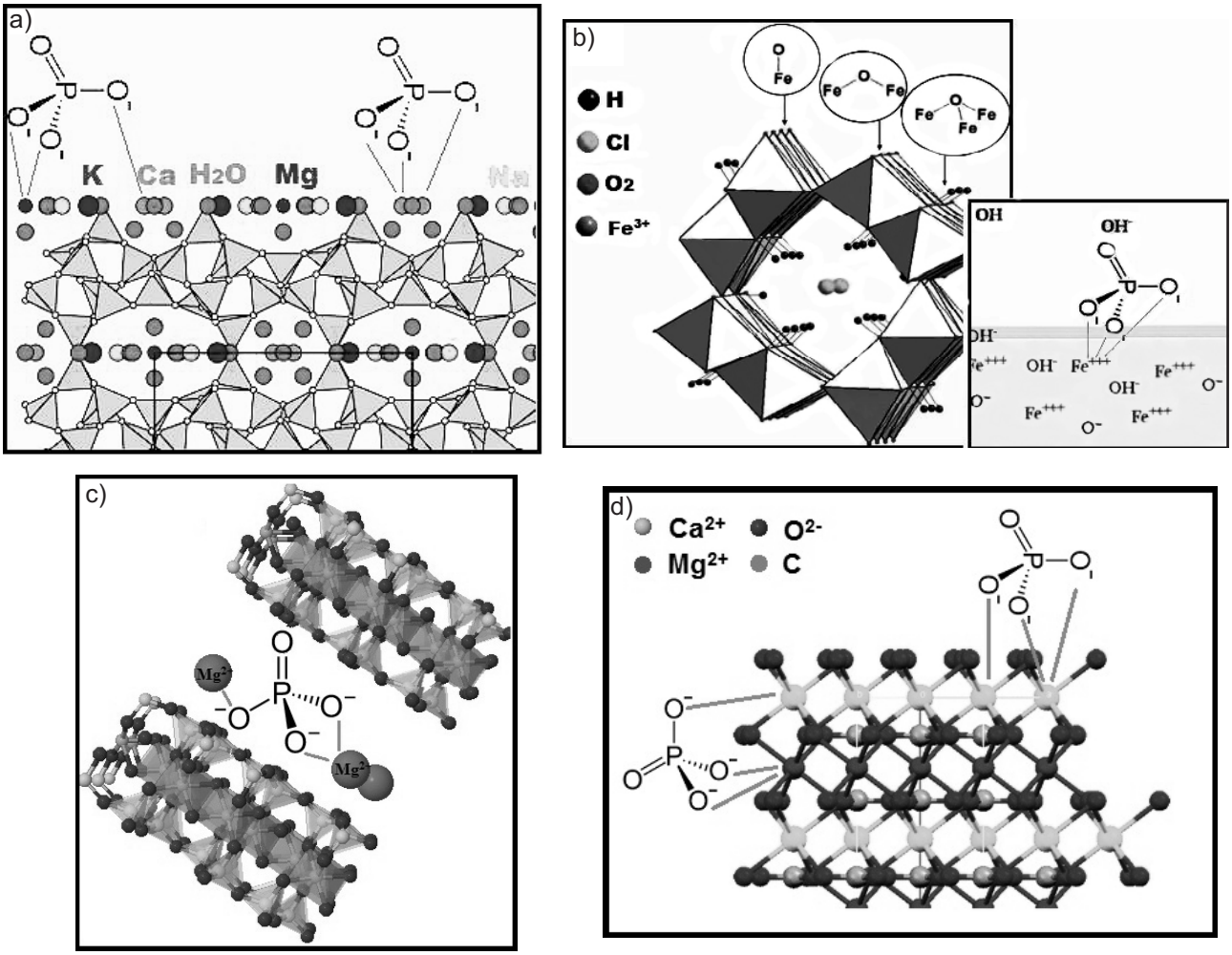

Fig. 9. Schematic illustration of the proposed: a) formation mechanism for $Ca_3(PO_4)_2$ and $Mg_3(PO_4)_2$ onto clinoptilolite-rich tuff, b) ionic bounds of the phosphate on the surface of oxyhydroxide GEH, c) phosphate intercalation mechanism into montmorillonite structure, d) phosphate covalent bounds onto slovakite surface.

structures (0.29×0.57 nm and 0.67×0.7 nm [17]), therefore phosphate adsorption by New Zeland mordenite-rich tuff was effective, too. Accessability and geometry of external pores as well as potential interparticle voids by natural zeolites, responsible for phosphate uptake performance, support also the fact resulting from chitosan-zeolite product examination, by which the phosphate adsorption substantially decreased, probably on the basis of external surface covering with chitosan chains.

Finally, to predict compatible bounding of phosphate onto the slag with the phosphate bounds onto zeolite, an elemental EDX-analysis of amorphous aluminosilicate slag was performed [17]. The results were compared to the clinoptilolite-rich tuff elemental analysis, respectively. Approximately twice higher content of CaO 8.95-9.9% and Fe_2O_3 4.12-5.17% in Chinese slag was determined than in the clinoptilolite-rich tuff. Clinoptilolite-rich tuff contained CaO in the range of 2.91-3.5% and Fe_2O_3 of 2-2.3%. Nevertheless, neither the higher content of Ca and Fe elements, nor the amorphous structure of the slag have been able to provide better adsorption.

Phosphate Elution Trials

The phosphate elution test into ammonium chloride solution out of the phosphate-loaded adsorbents, the procedure of which was described in the laboratory setup section, resulted in the easier desorption of strong precipitates of calcium and magnesium phosphates from clinoptilolite-rich tuff (a selectivity of clinoptilolite toward ammonium cations high probably enabled easier elution of Ca^{2+} [10, 18, 28]) than in the case of phosphate linked to the surface of GEH product, sensu stricto phosphate linked to Fe^{3+} of the akaganeite structure, as well as phosphate probably linked to the alkaline-earth cations of the slovakite structure. Desorption of phosphate out of the GEH product could be quantitatively estimated as about 3-times lower in regard to the phosphate desorption out of the clinoptilolite-rich tuff.

Conclusions

Based on the experimental results obtained in this study the following statements may be concluded:

Slovakian clinoptilolite rich tuff can be used effectivelly in the removal of phosphate ions from waters. Although montmorillonite, slovakite, and GEH[104] product proved slightly higher uptake capacities toward phosphate ions at the ambient temperature than the clinoptilolite-rich tuff did, the increased temperature of systems supported the uptake performance only by clinoptilolite-rich tuff, not by montmorillonite and GEH[104] adsorbents.

The film-diffusion is the rate-limiting step in all of the adsorbents examined, which simultaneously confirms the results of the applied Weber-Morris mass transfer model.

Energetically lower surface physisorption of phospate onto clinoptilolite-rich tuff, GEH, and montmorillonite, but chemisorption by slovakite was confirmed.

Under the standard conditions the adsorption of phosphate onto all adsorbents examined occurs spontaneously. The results of standard free energies indicate simultaneously that spontaneity slightly decreases with temperature.

Acknowledgements

This project was funded by the Slovak Scientific Council VEGA (Project No. 1/0185/12) and Slovak-Chinese Cooperation grant SK-CN-0033-12, for which the authors express their thanks.

References

1. DRAGAN E.S., DINU M.V. Removal of copper ions from aqueous solution by adsorption on ionic hybrids based on chitosan and clinoptilolite. Ion Exchange Lett. **2**, 15, **2009**.
2. YOON K.B., LEE E.A., JEON E., LEE Y.J. Process for preparing porous hybrid comprising zeolite and chitosan and porous hybrid prepared thereby. US Patent Application, Publ. No.: US 2006/ 0135360 A1, **2006**.
3. VANGRONSVELD J, STERCKX J., VAN ASSCHE F., CHIJSTERS H. Rehabilitation studies on an old non-ferrous waste dumping ground: effects of revegetation and metal immobilization by beringite. J. Geochem. Explor. **52**, 221, **1995**.
4. BABEL S., KURNIAWAN T.A. Low-cost adsorbents for heavy metals uptake from contaminated water: a review. J. Hazard. Mater. **B97**, 219, **2003**.
5. PITTER P. Hydrochemie, SNTL, Praha, 456, **2009**.
6. http://www.vurup.sk/products/molecularsieves/general/page1/slovak.html [accessed 2011-07-25].
7. VASS D., KONEČNÝ V., ELEČKO M., MILIČKA J., SNOPKOVÁ P., ŠUCHA V., KOZÁČ J., ŠKRABANA R. Alginite – a new resource of Slovak mineral potential (repository Pinciná). Mineralia Slovaca **29**, 1, **1997**.
8. RAJIC N., STOJAKOVIC D., JEVTIC S., ZABUKOVEC LOGAR N., KOVAC J., KAUCIC V. Removal of aqueous manganese using the natural zeolitic tuff from the Vranjska Banja in Serbia. J. Hazard. Mater. **172**, 1450, **2009**.
9. ZHOU Y. (Ed.) Bio-Inspired Nanomaterials and Nanotechnology. Nova Biomedical Books, New York, 301, **2010**.
10. INGLEZAKIS V.J., POULOPOULOS S.G. Adsorption, Ion Exchange and Catalysis: Design of Operations and Environmental Applications, Elsevier, Amsterdam, 602, **2006**.
11. LAGERGREN S. To Theory for so called Adsorption of Solutes. Kungl. Svenska vetenskapsakademiens handlingar, **24**, 1, **1898** [In German].
12. HO Y.S. Citation review of Lagergren kinetic rate equation on adsorption reactions Scientometrics **59**, 171, **2004**.
13. ALPAT S.K., OZBAYRAK O., ALPAT S., AKCAY H. The adsorption kinetics and removal of cationic dye, Toluidine Blue O, from aqueous solution with Turkish zeolite. J. Hazard. Mater. **151**, 213, **2008**.
14. ARGUN M.E. Use of clinoptilolite for the removal of nickel ions from water: Kinetics and Thermodynamics. J. Hazard. Mater **150**, 587, **2008**.
15. WEBER W.J. JR., MORRIS J.C. Removal of biologically resistant pollutants from waste waters by adsorption. In: Advances in Water Pollution Research, Pergamon Press, New York, pp. 231-266, **1962**.

16. SAMEŠOVÁ D., LADOMERSKÝ J. The contamination of surface water and soil in biosphere, Ekologia Ekologia **3**, 190, **2003**.
17. CHMIELEWSKÁ E., SABOVÁ L., GÁPLOVSKÁ K., ČAPLOVIČOVÁ M. Functionally graded mesoporous zeolitic adsorbents in order to promote the pollutants removal. Kuwait J. Sci. Eng. **35**, 1, **2008**.
18. www.zeocem.sk [accessed 2011-07-25].
19. www.geh-wasserchemie.de [accessed 2011-07-30].
20. GALAMBOŠ M., ROSSKOPFOVÁ O., KUFČÁKOVÁ J., RAJEC P. Utilization of Slovak Bentonites in deposition of high-level radioactive waste and spent nuclear fuel. J. Radioanal. Nucl. Ch. **288**, 765, **2011**.
21. HO Y.S., MCKAY G. Sorption of dye from aqueous solution by peat. Chem. Eng. J. **70**, 115, **1998**.
22. HO Y.S. Review of second-order models for adsorption system. J. Hazard. Mater. **136**, 681, **2006**.
23. WEBER W.J. JR., MORRIS J.C. Kinetics of adsorption on carbon from solution. J. Sanitary Eng. Div. – ASCE **89**, 31, **1963**.
24. MICHELSON L.D., GIDEON P.G., PACE E.G., KUTAL L.H. Removal of soluble mercury from wastewater by complexing technique. US Dept Industry, Office of the Water Research and Technology, Bull. No. 74, **1975**.
25. HONG S., WEN CH., HE J., GAN F., HO Y. Adsorption thermodynamics of Methylene Blue onto bentonite. J. Hazard. Mater. **167**, 630, **2009**.
26. BHATTACHARYYA K.G., GUPTA S.S. Adsorption of a few heavy metals on natural and modified kaolinite and montmorillonite: A review. Adv. Colloid Interfac. **140**, 114, **2008**.
27. YAN L., XU Y. YU H., XIN X., WEI Q., DU B. Adsorption of phosphate from aqueous solution by hydroxy-aluminum, hydroxy-iron and hydroxy-iron-aluminum pillared bentonites. J. Hazard. Mater. **179**, 244. **2010**.
28. TOMEČKOVÁ V., REHÁKOVÁ M., MOJŽIŠOVÁ G., MAGURA J., WADSTEN T., ZELENÁKOVÁ K. Modified natural clinoptilolite with quercetin and quercetin dihydrate and the study of their anticancer activity. Micropor. Mesopor. Mater. **147**, 59, **2012**.
29. BARBALACE K. Periodic Table of Elements – Sorted by Ionic Radius. Environmental Chemistry.com, 1995-2010 http://klbprouctions.com (accessed 2010-7-03).
30. ŠERŠEŇ F., PAVLÍKOVÁ S., JESENÁK K., SZÖCS V., ČÍK G. Effect of methylene blue and chlorophyllin embedded in natural zeolite on algae growth in medium polluted by chlorophenol. Fresenius Environ. Bull. **20**, 2271, **2011**.
31. GALAMBOŠ M., SUCHÁNEK P., ROSSKOPFOVÁ O. Sorption of anthropogenic radionuclides on natural and synthetic inorganic sorbents. J. Radioanal. Nucl. Chem. **293**, 613, **2012**.